JOM, Vol. 76, No. 2, 2024
https://doi.org/10.1007/s11837-023-06276-6

Effect of Cu Doping on Structural, Optical, and Electrical Properties of Sn_2S_3 Thin Films Prepared by Spray Pyrolysis

B.S. NAGARAJA,[1] K.P. GIRIJA,[2] K. MAHENDRA,[3,7] JAYADEV PATTAR,[3,8] S.C. GURUMURTHY,[4] RAVIKIRANA,[5] ASHOK RAO,[6] and K. SHYAM PRASAD[1]

1.—Department of Physics, Nitte (Deemed to be University), NMAM Institute of Technology (NMAMIT), Nitte, Karkala, Karnataka 574110, India. 2.—Department of Mathematics, Nitte (Deemed to be University), NMAM Institute of Technology (NMAMIT), Nitte, Karkala, Karnataka 574110, India. 3.—Department of Physics, School of Applied Sciences, REVA University, Bengaluru, Karnataka 560064, India. 4.—Nanomaterials and Polymer Physics Lab, Department of Physics, Manipal Institute of Technology, Manipal Academy of Higher Education, Manipal, Karnataka 576104, India. 5.—Department of Physics and Nanotechnology, SRM Institute of Science and Technology, Kattankulathur, Tamilnadu 603203, India. 6.—Center for Clean Energy, Department of Physics, Manipal Institute of Technology, Manipal Academy of Higher Education, Manipal 576104, India. 7.—e-mail: manukolya@gmail.com. 8.—e-mail: jayadev.pattar@gmail.com

The structural, optical, morphological, and electrical properties of polycrystalline copper-doped tin sulfide (Cu-Sn_2S_3) thin films with different concentrations of Cu dopants were synthesized using the spray pyrolysis method. Structural characterizations (powder XRD) revealed orthorhombic Sn_2S_3 crystal structure with *Pmma* space group. The XRD spectra showed improved crystalline quality and preferential orientation for the Cu-doped Sn_2S_3 thin films. Morphology of the prepared samples revealed sharp needle-shaped grains uniformly distributed throughout the sample. The UV spectroscopy results show 70–75% transmittance for 6 wt.% and 8 wt.% Cu-doped Sn_2S_3 thin films in the visible region. The bandgap values are decreased for the 4 wt.% sample and increased with an increase in the Cu concentration for 2 wt.%, 6 wt.%, and 8 wt.% with Sn_2S_3 thin films. The dielectric constant, dielectric loss, and electrical and optical properties were analyzed using UV data. Negative Hall coefficient values of prepared samples confirm the *n*-type semiconductor nature. Electrical conductivity increases with an increase in Cu concentration. These results indicate that the samples have potential applications in the optoelectronic field.

INTRODUCTION

In recent years, chalcogenide semiconducting thin films such as tin sulfide (SnS), SnS_2, and Sn_2S_3 have gained attention because of their physical and chemical properties. These properties are more favorable to potential applications in photovoltaic and optoelectronic devices.[1–4] Among these, Sn_2S_3 thin films turned out to be the most promising material of the IV–VI group of semiconductors, which crystallizes in orthorhombic crystal structure.[1,5–7] The Sn_2S_3 thin films exhibit *n*-type conductivity with a direct bandgap that lies between 0.9 eV and 2.2 eV.[7,8] The observed high values of the direct band gap of 2.8–2.9 eV range can be used for the buffer layer of solar cells.[9] Therefore, Sn_2S_3 thin films reported various band gap energies with an anisotropic conduction nature which can be used for suitable semiconductor materials for building photovoltaic *p–i–n* or *p–n* structure.[10] The Sn_2S_3 thin film shows an electrical resistivity of 0.864 Ω cm at an energy band gap of 1.06 eV.[11] The conductivity in Sn_2S_3 thin films

(Received May 28, 2023; accepted October 31, 2023; published online November 21, 2023)

mainly depends on Sn vacancies, which can act as acceptor defects, and electron traps can be created due to the vacancy of S. Sn_2S_3 single-phase films would be interesting to determine the transport properties by controlling the Sn and S vacancies, which can be used for photovoltaic applications. In addition to being highly conductive and transparent, ITO-Sn_2S_3 films were effectively sensitive to visible light and can be of use in developing photoconductive sensors.[12] Sn_2S_3 thin films were also studied for dielectric constant, carrier concentration, effective mass, and plasma frequency.[8,12] The complex dielectric constant is directly related to the deposition time. Therefore, the deposition time significantly influences the structural and optical properties of Sn_2S_3 thin films.[2] To achieve single-phase Sn_2S_3 thin film, it is important to control the self-compensation effect of sulfur vacancies, which can be achieved through doping. Doping with elements such as accepter-type impurities can enhance photo-response characteristics.[13–16] Notably, Cu doping with CdS, ZnO, and SnS compounds shows a reduction in its photocurrent and high-value conductivity in *p*-type semiconductors.[14,16–19] The formation of Sn_2S_3 films is usually in the form of interconnected spherical particles because of the presence of various boundaries of particles[19] which can create low electron-transport efficiency due to which electron-hole recombination is achieved, thereby reducing the efficiency of solar cells and other applications.[10] Cu doping has increased the acceptor carrier concentration; in Cu:SnS/In_2S_3 heterojunction devices, > 462 mV VOC (in the device) is achieved, which is more than double than that of the un-doped case. The Cu-doped Sn_2S_3 thin film revealed the minimum resistivity for 2 wt.% Cu concentration and exhibited improved physical properties. Semiconductor doping thus has great importance in optoelectronic device applications. The Sn_2S_3 thin films can be prepared using various techniques such as chemical vapor deposition,[20] thermal evaporation,[21] electrochemical deposition,[13] molecular beam epitaxy,[3] SILAR,[22] and spray pyrolysis.[23] Among these deposition techniques, one of the most significant techniques is spray pyrolysis; it can be used to deposit thin film using a glass substrate, which is very simple, more flexible, inexpensive, and capable of producing large-area coating. The reports on Cu-doped Sn_2S_3 thin films are sparse, and there is a huge scope to understand the properties of Sn_2S_3 thin films under the influence of Cu. In this regard, the present investigation author synthesized Sn_2S_3 thin film using spray pyrolysis technique with different doping concentrations of Cu (x = 0 wt.%, 2 wt.%, 4 wt.%, 8 wt.%) and explored the structural, optical, and dielectric properties of Cu on Sn_2S_3 thin films.

EXPERIMENTAL PART OF CU-DOPED SN_2S_3

Sample Preparation

The Cu-doped Sn_2S_3 thin films were deposited using the spray pyrolysis technique on a glass substrate. Initially, the glass substrates were thoroughly cleaned using deionized (DI) water followed by isopropyl alcohol and acetone successively. Chemicals of analytical grade are used to synthesize the desired thin films. The solution of 0.1 M $SnCl_2.2H_2O$ and 0.1 M *N*,*N*-dimethyl thiourea was dissolved in 400 ml deionized water. Furthermore, 10 ml hydrochloric acid was added to the total volume of 400 ml, and then the solution was well mixed using a magnetic stirrer for nearly 2 h maintaining a constant temperature of 60 °C. The 0.1 M of copper chloride ($CuCl_2$) solution was used as the dopant, doping with 2 wt.%, 4 wt.%, 6 wt.%, and 8 wt.% Cu concentrations. The substrate temperature was kept at 350 °C, and the solution flow rate was maintained at 1 ml/min. The substrate to the substrate distance was kept at about 16 cm, and 2 ml min^{-1} gas pressure was maintained. Furthermore, after completion of the deposition process, the thin films were annealed at 350 °C.

Characterization Techniques

The prepared thin films were characterized to study their structural and physical properties. The structural properties were characterized using XRD (Bruker's) source of 1.5406 Å wavelength. The surface morphology of prepared thin films was analyzed by using high-resolution scanning electron microscopy (HR-SEM). The optical properties like absorption coefficient, transmittance, and optical energy bandgap (E_g) were determined using a Cary 5000 UV-visible-NIR spectrophotometer. Hall coefficient, mobility, and carrier concentration were quantified using the Ecopia HMS-5500 Hall effect measurement system by the Van der Pauw technique.

RESULTS AND DISCUSSION

Structural Properties

Figure 1 shows the observed major reflections of XRD patterns corresponding to the orthorhombic Sn_2S_3 crystal structure with *Pnma* space group (ICCD No. 00-030-1377). The presence of a peak indicates polycrystalline nature with preferential orientations along the (211) planes. No additional peaks were identified that corresponded to the other sulfides of tin, which implies the deposition of thin films has single-phase Sn_2S_3 without any phase segregation. The observed results were well matched with those of other researchers.[7,16] The plane (2 1 1) intensity increased for 2% of Cu doped with Sn_2S_3 thin films, which confirms its improved crystallinity. Thereafter, the observed intensity is decreased by increasing the concentration of Cu

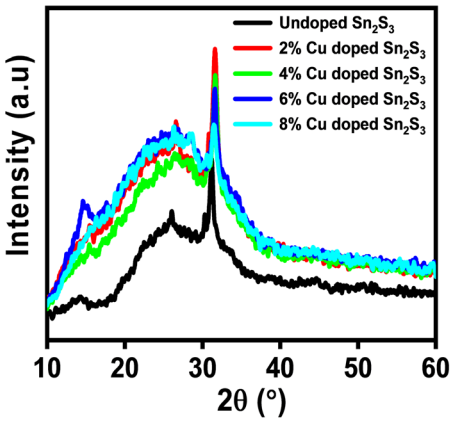

Fig. 1. XRD patterns of pure and Cu-doped Sn_2S_3 thin films.

from x = 0.4–0.8% with Sn_2S_3 thin films. Several factors may lead to a slight decrease in crystalline quality: (1) saturation of the formation of newer nucleation centers; (2) when more Cu^{2+} ions enter Sn^{2+} lattice sites, lattice distortion intensifies, which leads to greater strain in the films, which affects grain growth.[24] Notably, peaks are shifted to a higher angle side up to 4 wt.% Cu-doped thin films, and the peak shifts towards a lower angle side for the 6 wt.% and 8 wt.% Cu-doped Sn_2S_3 thin films. These results suggest that the lattice parameter values are changing with an increase in the concentration of Cu in Sn_2S_3 thin films. The intensity of the XRD peak for the doped films has been considerably reduced compared to the pure Sn_2S_3, and this can be ascribed to the replacement of the smaller Cu^{2+} ions (0.73 Å) by larger Sn^{2+} (0.93 Å) ions at the cationic site. This causes internal stress in the crystal lattice without affecting the crystal structure in a significant way. Doped films exhibit increased crystallinity for a dopant concentration of 4 wt.%, and as the dopant concentration is increased, the film's crystallinity decreases.

Lattice parameters are calculated using the following formula:

$$\frac{1}{d^2_{(hkl)}} = \frac{h^2}{a^2} + \frac{k^2}{b^2} + \frac{l^2}{c^2} \tag{1}$$

The values are tabulated in Table S1 (Supplementary content), showing that the lattice parameters a and b decreased for 2 wt.% compared to pure, then they increased for 4 wt.%. Later, they show an the increasing trend with Cu doped with Sn_2S_3 thin films. For the parameter $\boldsymbol{c}$ shows variation in values with Cu doping. The volume of Cu-doped Sn_2S_3 thin films is observed to decrease for 2 wt.% Cu doped; then, it increases with increasing concentration of Cu in Sn_2S_3 thin films. This might be caused by the presence of a defect within the crystal's cell, which results in local changes in the crystalline structure and their lattice parameters.

From the x-ray patterns, the crystalline size (D) for the prepared thin films has been calculated using Scherrer's formula. The dislocation density (δ), lattice strain (ε) associated with lattice mismatch, and the number of crystallites (N) per unit volume are evaluated using the following formulae.[11,24,25]

$$D = \frac{0.9\lambda}{\beta \cos\theta} \tag{2}$$

$$\delta = {}^{1}\!/_{D^2} \tag{3}$$

$$\eta = \frac{\beta \mathrm{Cos}\theta}{4} \tag{4}$$

$$N = \frac{t}{D^3} \tag{5}$$

where θ is the Bragg's angle, β is the full width at the half maximum (FWHM), and λ is the wavelength of the X-rays. Table S1 (Supplementary content) represents the variation of calculated parameters of Cu-doped Sn_2S_3 thin films. The crystalline size is decreased for 2 wt.% Cu, sample, and it is increased for 4 wt.% Cu-doped thin films. Again, it decreased for 6 wt.% and 8 wt.% Cu-doped thin films compared with pure Sn_2S_3 thin films. Thin films prepared from Cu^{2+} ions replace the larger Sn^{2+} ionic site with the smaller Cu^{2+} ion, as illustrated by the reduced crystallite size compared with pure Sn_2S_3. The decrease in crystal size can be explained based on Vegard's law.[26] A uniform crystal contraction occurs when the substitution atoms (Cu^{2+}) of a smaller radius than the host (Sn^{2+}) atoms are present and are proportional to their concentration. As a result of a smaller grain size, a smaller barrier height reduces the recombination speed at grain boundaries. Consequently, reduced crystal size will reduce the grain boundary scattering of charge carriers, which results in a larger surface-to-volume ratio, which further influences the structural and optical properties of film samples. For the 4 wt.% concentration sample, the increased crystal size may be due to either agglomeration of Cu clusters or occupation at the interstitial sites. In addition, the Cu has a greater affect on Sn_2S_3 film, which can increase the lattice defect, and the result may cause the variation in the dislocation density (δ), lattice strain (ε), and number of crystallites (N) per unit volume values in these thin films. The observed data show that Cu doping to Sn_2S_3 can profoundly alter the structural properties of Sn_2S_3 thin films.

Morphology

The surface morphology of pure Sn_2S_3 and doped with Cu was studied using Hi-resolution scanning electron microscopy (HR-SEM) and is shown in Fig. 2. Figure 2a–e shows the clearly distinguished variation of morphology in the film because of the

effect of Cu ion in Sn_2S_3 thin films. On the smooth surface, flattened sharp needle-shaped grains distributed without any voids are present in pure Sn_2S_3 and 2 wt.% Cu-doped Sn_2S_3 thin films. For the 4 wt.% Cu doped Sn_2S_3 thin film, densely packed sharp needle-shaped grains are observed. The surface shows the agglomeration and coalescence of sharp needles present in some parts for the 6 wt.% Cu-doped Sn_2S_3 thin films. For the 8 wt.% Cu-doped Sn_2S_3 thin film grains appear in the spherical with the smallest size. A similar type of morphology for Sn_2S_3 thin films has been already reported.[1,7,15,16,24,27] Thus, the film morphology confirmed that prepared films are modified with Cu-doped Sn_2S_3 thin film from flattened sharp-needled grains to small spherical grains with Cu doping.

OPTICAL PROPERTIES

Figure 3a shows the optical absorption spectrum of thin Sn_2S_3 films with and without Cu doping. Absorbance decreases with increasing wavelength for the entire region. In all the films, a sharp absorption edge is observed, which is like the behavior of semiconductor films. It is apparent from the inset in Fig. 3a that 2 wt.% and 4 wt.% doped films exhibit an increased absorbance value compared to pure films in the range of 350–600 nm, possibly because of defects introduced by doping. Furthermore, as Cu concentration increases in Sn_2S_3 thin films at higher wavelengths, the absorbance decreases because of the film's crystalline size. Figure 3a shows that absorbance decreases with increasing concentration for the entire wavelength for 6 and 8 wt.% Cu-doped Sn_2S_3 thin films.

Figure 3b shows the % transmittance spectra of Cu-doped Sn_2S_3 thin films in the range of 300–2400 nm. The transmittance is decreased for 2 and 4 wt.% whereas it increased for 6 and 8 wt.% Cu-doped Sn_2S_3 thin film in the wavelength range 300–650 nm. The transmittance is observed as nearly 70–72% for pure and 2 wt.% doped, 70–75% for 6 wt.% and 8 wt.% doped thin films, and 61–67% for 4 wt.% doped thin films in the higher wavelength range. These results suggest that for the small ionic radius of Cu ions compared to Sn ions, Cu ions have a more significant effect on Sn_2S_3 thin films.

Absorption and extinction coefficients are the most important factors in optical analyses, which can be estimated by absorbance and reflectance values across the entire wavelength range in optical studies. Therefore, the equation $\alpha = 2.303A/t$ can be used to estimate the absorption coefficient (α) by using the data of measured absorbance (A), and t is the prepared thin film thickness (i.e., t = 460 nm). Figure 4b shows that at lower wavelengths the value of α decreases near the band edge for all the thin films. The extinction coefficient of the Cu-doped Sn_2S_3 thin film is calculated using the formula $k = \alpha\lambda/4\pi$[11] and is plotted as shown in Fig. 4a. It is noticed that doped Sn_2S_3 thin films exhibit extinction coefficient values ranging from 0.38 to 0.10. These low extinction coefficient values suggest the low surface roughness of the film.

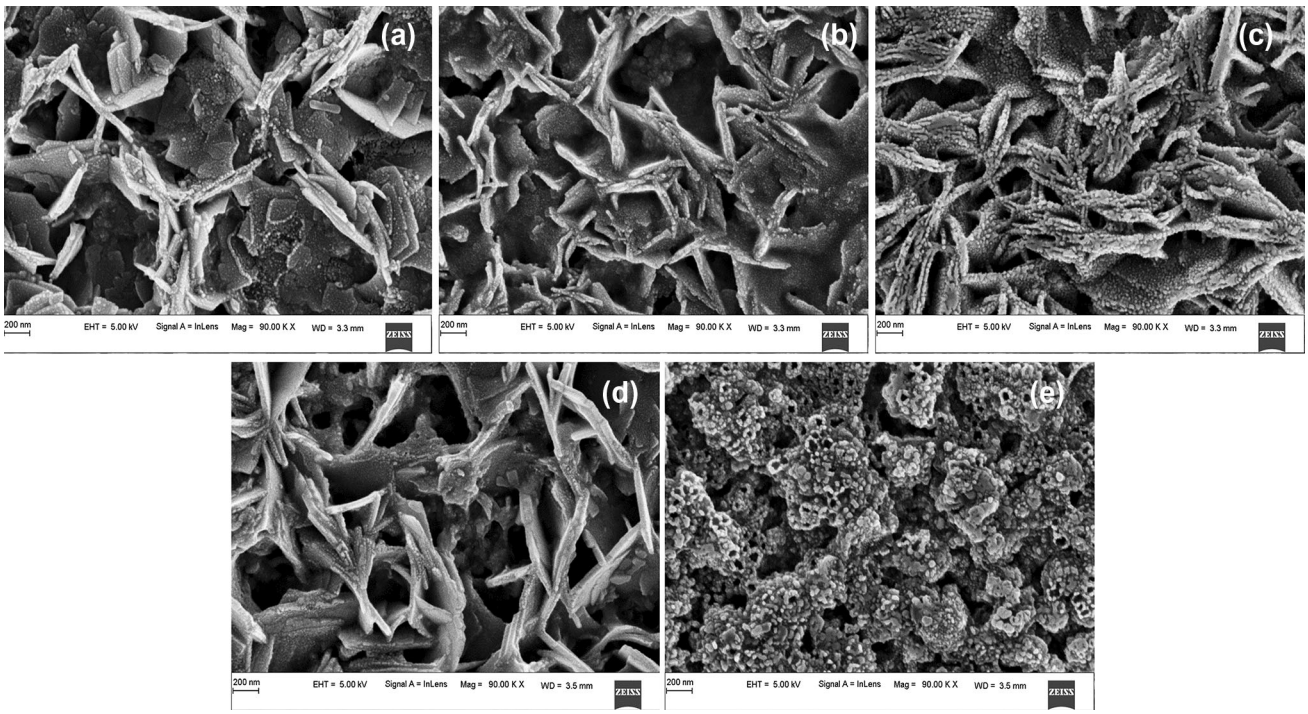

Fig. 2. SEM images of (a) pure Sn_2S_3, (b) 2% Cu-doped Sn_2S_3, (c) 4% Cu-doped Sn_2S_3, (d) 6% Cu-doped Sn_2S_3, and (e) 8% Cu-doped Sn_2S_3 films.

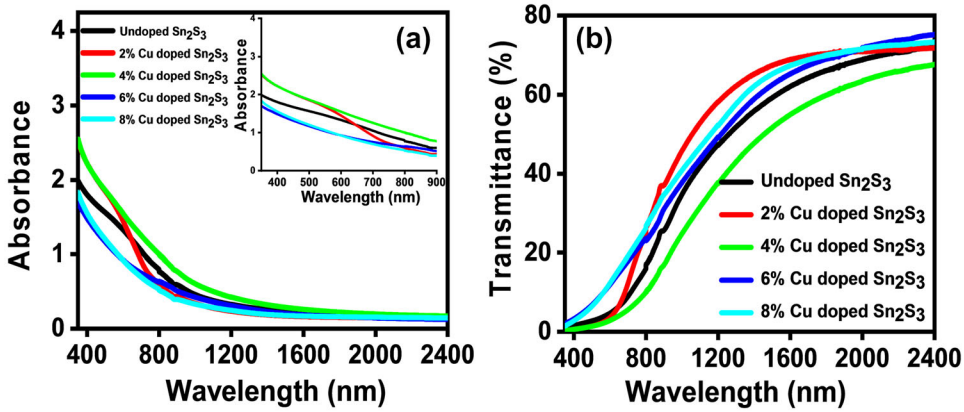

Fig. 3. Plots of (a) absorbance and (b) transmittance for pure and Cu-doped Sn_2S_3 films.

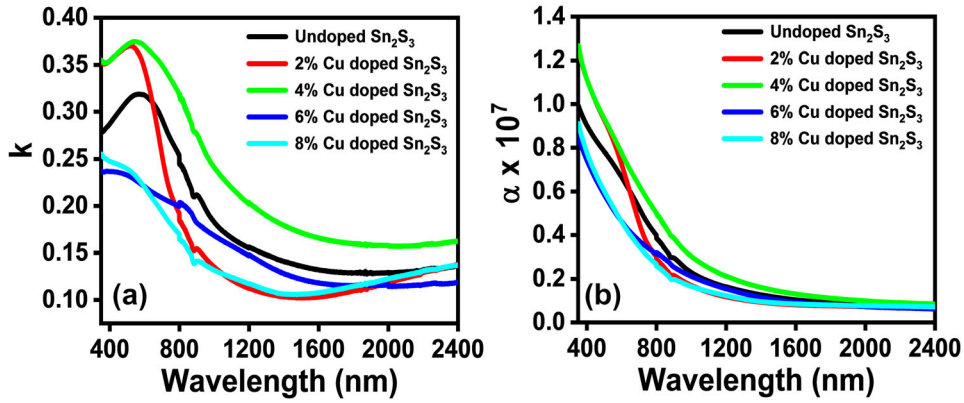

Fig. 4. Variation of (a) extinction coefficient (k) and (b) absorption coefficient (α) for pure and Cu-doped Sn_2S_3 thin films.

The energy bandgap of Cu-doped Sn_2S_3 thin films is evaluated from the relations $\alpha h\nu = A(h\nu - E_g)^m$, where A is a proportionality constant, E_g represents the energy bang values, h is Planck's constant, and ν is photon frequency. Also, m value is a constant that depends on the type of transition, and for the direct transition m value is 1/2; for the indirect transition m value is 2. The curve $(\alpha h\nu)^{1/2}$ for the indirect transition does not support linearity. This suggests that Cu-doped Sn_2S_3 has a direct bandgap, and it is shown in Fig. 5a. The energy band gap values were obtained by extrapolating the linear behavior of $(\alpha h\nu)^2$ versus the photon energy $(h\nu)$ plot. The estimated value of the energy band gap is tabulated in Table S1 (Supplementary content). The observed result of pure Sn_2S_3 thin film is in good agreement with reported values.[16,21,28,29] The observed band gap values decrease for Sn_2S_3 thin films doped with 2 wt.% Cu and then increase slightly for higher Cu doping concentrations. An increase in carrier concentration can lead to a reduction in the energy band gap due to the band shrinkage effect.[16,23] Also, there may be volatility in the Sn/S stoichiometry ratio, which can induce lattice defects in the films. An increase in the energy band for higher concentration is due to the effective incorporation of Cu-dopant into the Sn_2S_3 lattice since Cu ions are well replaced with Sn ions, which can enhance the value of the band gap.[16,29] Therefore, these results confirm that Cu is more effective in the properties of Sn_2S_3 thin films.

The Cu-doped Sn_2S_3 thin film refractive index values were calculated using the Fresnel formula for pure and Cu-doped Sn_2S_3.[13,30,31]

$$n = \frac{1 + R^{0.5}}{1 - R^{0.5}} \tag{6}$$

The refractive index of the Cu-doped Sn_2S_3 thin films with variation of wavelength are presented in Fig. 5b. The observed value of the refractive index is found to be increasing with doping Cu up to 4 wt.% and decreased for 6wt.% and 8 wt.% in the UV-visible range. The value of the refractive index decreases with an increased wavelength from 650 nm to 1100 nm for all the samples. Furthermore, the values increase with the increase in the wavelength. These behaviors are because of encumbering the Sn_2S_3 thin film, and it may be due to the porosity in the films. The observed values vary from 1.45 to 1.31 in the visible region, and the refractive index is increasing with increasing wavelength.

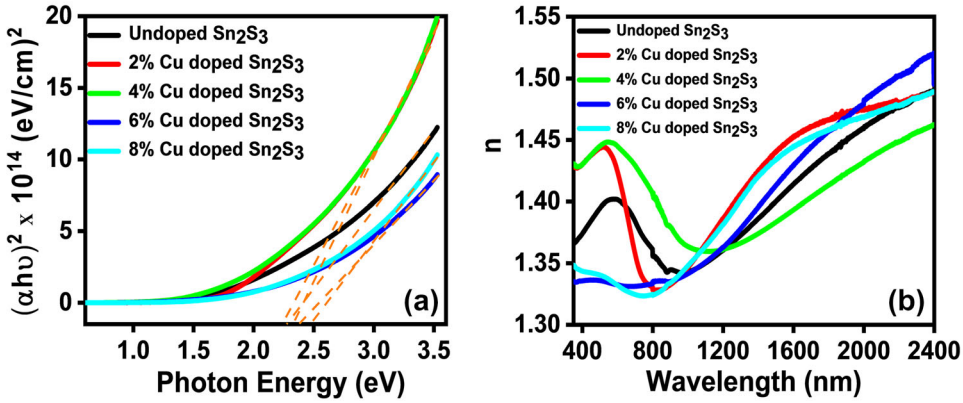

Fig. 5. Variation of (a) direct energy bandgap and (b) refractive index (n) for pure and Cu-doped Sn_2S_3 thin films.

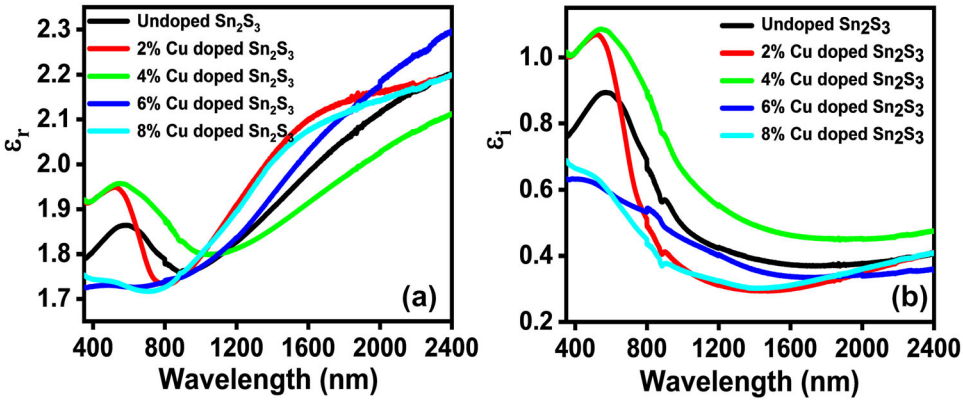

Fig. 6. Plots of (a) real and (b) imaginary parts for pure and Cu-doped Sn_2S_3 thin films.

The values of the real and imaginary part of the dielectric constant along with loss tangent were calculated for Cu-doped Sn_2S_3 thin films. Their constraints are extremely applicable for significant applications of thin films in dynamic random access memory (DRAM) and capacitive storage devices.[32,33] The real and imaginary parts of the dielectric can be determined using the value of n and k from the following relation[18,25,34] and are shown in Fig. 6a and b.

$$\varepsilon_r = n^2 - k^2 \tag{7}$$

$$\varepsilon_i = 2nk \tag{8}$$

The real part values are more than those of the imaginary part values of Cu-doped Sn_2S_3 thin films. These results suggest that the good quality of the grown film and its improved optical properties can be highly suitable for optoelectronic applications.

The dielectric loss tangent ($\tan\delta$) values can be estimated for all the samples using the following equation and are shown in Fig. 7.

$$\tan\delta = \frac{\varepsilon_i}{\varepsilon_r} \tag{9}$$

As wavelength increases, the tangent values decrease, and a sharp decrease in dielectric loss can be observed between 450 nm and 650 nm while remaining constant at higher wavelengths. These results suggest that the photons and electrons are interacting at shorter wavelengths in thin films.

The rate at which electrons lose energy through materials is a significant factor in determining dielectric constants. This can be explained based on the surface energy loss function (SELF) and volume energy loss function (VELF). It is possible to calculate these parameters using the real and imaginary parts of the dielectric constant, which can be calculated as follows.[35,36]

$$\mathrm{VELF} = -\mathrm{Im}\left(\frac{1}{\varepsilon}\right) = \frac{\varepsilon_i}{\varepsilon_r^2 + \varepsilon_i^2} \tag{10}$$

$$\mathrm{SELF} = -\mathrm{Im}\left(\frac{1}{\varepsilon + 1}\right) = \frac{\varepsilon_i}{(\varepsilon_r + 1)^2 + \varepsilon_i^2} \tag{11}$$

The observed values of SELP and VELF with the function of wavelength are shown in Fig. 8a and b. The values of SELF and VELF decrease with an increasing wavelength indicating a reduction in the

electron energy loss at a higher wavelength. The main reasons for nearly identical behavior between VELF and SELF are the traveling of free charge carriers through the surface and volume. Therefore, these results confirm the inelastic scattering of electrons within the framework of the dielectric theory. However, these films experience greater volumetric energy loss as a function of wavelength than surface energy loss.

The optical absorption coefficient and refractive index values are used to estimate the optical (σ_{opt}) and electrical conductivity (σ_{ele}), and these parameters can be determined by using the following relations.[36,37]

$$\sigma_{opt} = \frac{\alpha n c}{4\pi} \tag{12}$$

$$\sigma_{ele} = \frac{2\lambda\sigma_{opt}}{\alpha} \tag{13}$$

The optical and electrical properties as a function of wavelength using the speed of light (3×10^8 m/s) were calculated and are shown in Fig. 9a and b. The σ_{opt} value decreases with increasing wavelength, as shown in Fig 9a. Figure 9b shows that σ_{ele} increases with wavelength, which suggests that thin films of Cu-doped Sn_2S_3 show better conductivity. The results suggest that the enhanced conductivity is observed because of a reduction of grain boundaries caused by dopants influencing charge carriers.

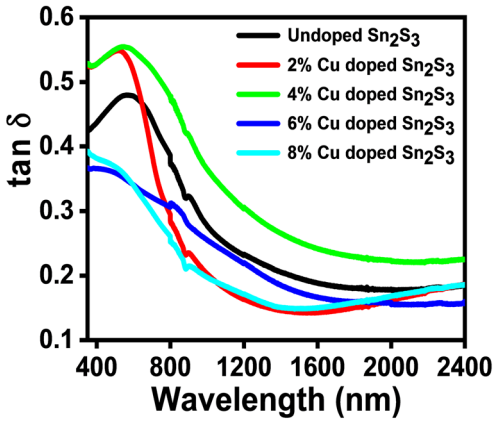

Fig. 7. Dielectric loss values for pure and Cu-doped Sn_2S_3 thin films for different wavelengths.

Non-linear Optical Studies

As thin films exhibit good nonlinear polarizability, nonlinear susceptibility of second and third orders is extremely important in optoelectronic applications. Whenever the suitable incident light interacts with a display device, a nonlinear refractive index can be used as a measure of the display device's light-gathering capability. The following equations can be used to determine nonlinear polarizability (P_{NL})[36–39]

$$P = \chi^{(1)}E + P_{NL} \tag{14}$$

where $P_{NL} = \chi^{(2)}E^2 + \chi^{(3)}E^3$, the polarizability can be represented by P, the second order is $\chi^{(2)}$, and the linear optical susceptibility is $\chi^{(1)}$. The linear refractive index $n(\lambda)$ can be calculated using following equation.[36–39]

$$n(\lambda) = n_0(\lambda) + n_2(E^2) \tag{15}$$

where $n_0(\lambda)$ is the intensity-dependent linear and $n_2(\lambda)$ is nonlinear refractive index.

The value of $n(\lambda)$ can be expressed as $n_0(\lambda) \gg n_2(\lambda)$. Therefore, the mean square of the electric field is written as $n(\lambda) = n_0(\lambda)$. The value of linear optical susceptibility $\chi^{(1)}$ can be calculated using n values based on the following relation.

$$\chi^{(1)} = (n^2 - 1)/4\pi \tag{16}$$

Based on the linear optical susceptibility, the $n_0(\lambda)$ and third-order nonlinear optical susceptibility can be calculated as follows.

$$\chi^{(3)} = A\left(\chi^{(1)}\right)^4 \tag{17}$$

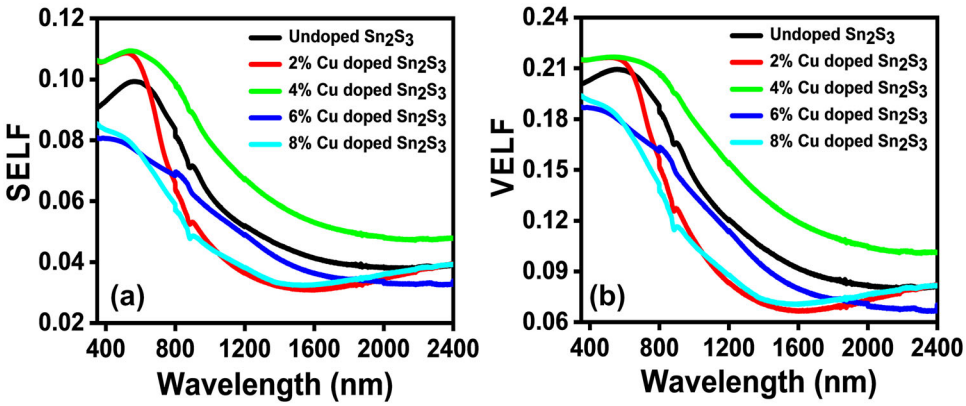

Fig. 8. Plots of (a) SELF and (b) VELF for pure and Cu-doped Sn_2S_3 thin films.

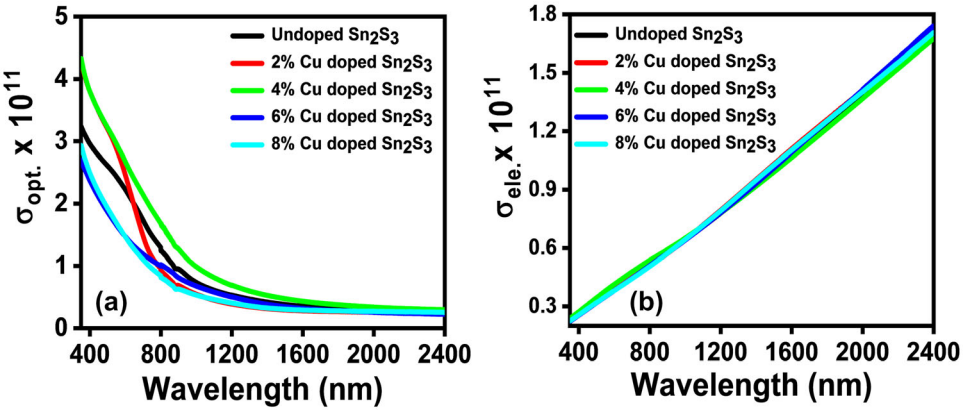

Fig. 9. Variation of (a) optical conductivity and (b) electrical conductivity of pure and Cu-doped Sn_2S_3 thin films.

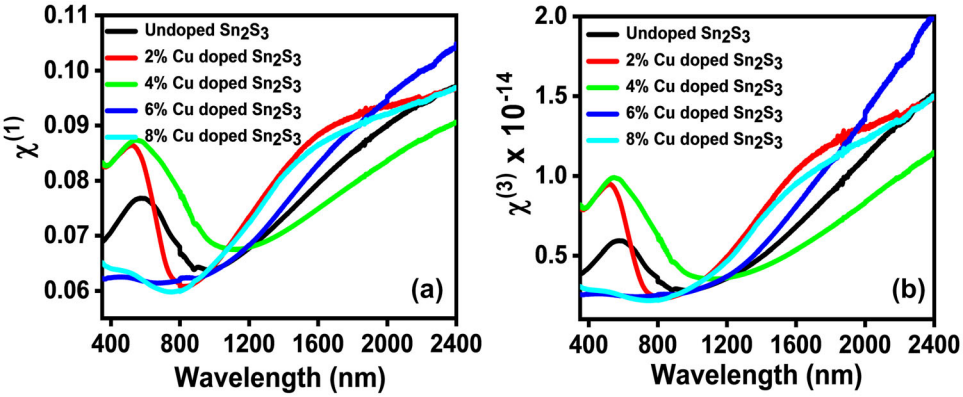

Fig. 10. Variation of (a) linear susceptibility $(\chi^{(1)})$, (b) third order nonlinear susceptibility $(\chi^{(3)})$ of pure and Cu-doped Sn_2S_3 thin films.

The above Eq. 17 can be modified using the Eq. 16, and it can express as follows.

$$\chi^{(3)} = \frac{A}{(4\pi)^4}\left(n_0^2 - 1\right)^4 \tag{18}$$

where the value of A is constant (i.e., $A = 1.7 \times 10^{-10}$ esu.) Therefore, a simple equation can be used to determine the non-linear refractive index

$$n_2 = \frac{12\pi\chi^{(3)}}{n_0} \tag{19}$$

Figure 10a and b shows the linear and third-order nonlinear susceptibilities of Sn_2S_3 with doping of Cu and pure Sn_2S_3 as a function of wavelength. Figure 11 shows the nonlinear refractive index of Sn_2S_3 with Cu doping as a function of wavelength. As can be seen, linear and third-order nonlinear susceptibility values show similar behavior as nonlinear refractive index values, which are also the same as refractive index values. The observed pure and Cu-doped Sn_2S_3 samples results of $\chi^{(1)}$, $\chi^{(3)}$, and n_2 were found to be in the range from 0.059 to 0.104 esu., 2.4×10^{-15}–2×10^{-14} and 6.20×10^{-14}–4.99×10^{-13}, respectively. It can be concluded that Cu is more significantly affected by Sn_2S_3 thin films, and these results can be applied to nonlinear optical applications.

ELECTRICAL PROPERTIES

Hall Effect

The Hall effect measurement is performed at room temperature for prepared thin films. From the Hall measurements, we can observe conductivity (σ), resistivity (ρ), Hall coefficient (R_H), mobility (μ), and charge carrier density (n). All observed values are presented in Table S2 (Supplementary content). Hall coefficient values indicate the negative sign, which suggests the n-type semiconductor behavior.[8,24] From Table S2 (Supplementary content), the resistivity is increased for 2 wt.% Cu-doped Sn_2S_3 thin film; thereafter, the resistivity decreases with increases in the concentration of Cu in Sn_2S_3 thin films. For the 2 wt.% Cu doping, the resistivity increased because of scattering of grain boundary effect to the thin films, and observed results have smaller grain size and volume compared to pure and higher doping of Cu concentration.[23,29,30] From Table S2 (Supplementary content) resistivity and mobility values are increasing with increasing Cu

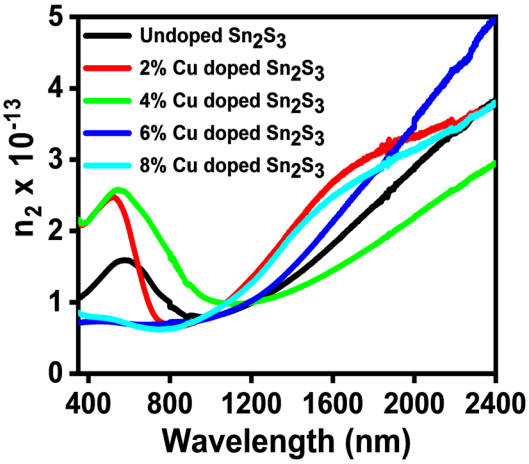

Fig. 11. Variation of nonlinear refractive index (n_2) with function of wavelength of pure and Cu-doped Sn_2S_3 thin films.

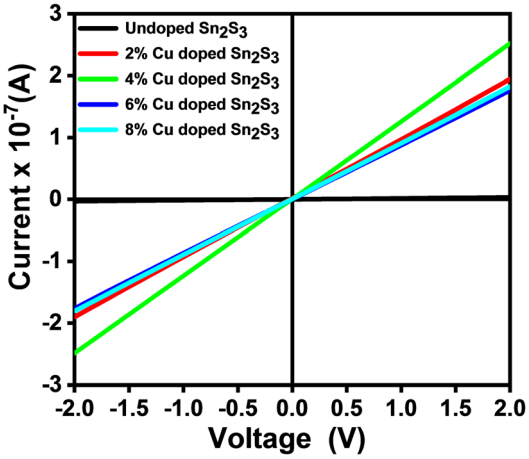

Fig. 12. I–V characteristic curve for pure and Cu-doped Sn_2S_3 thin films.

concentration from 4 wt.% to 8 wt.% Cu concentration in Sn_2S_3 thin films. This can be attributed to the presence of Cu ion in the replacement of Sn ion sites which leads the carrier concentration, and results will increase the electrical conductivity or decrease the resistivity. In addition, Cu ions in Sn sites can create sulfur vacancies, resulting in an increased concentration of carriers for every Cu addition.[6,7,29] In thin films, the inter-granular effect may play a significant role in the transport of carriers, which may explain the decrease in charge carrier concentration for the Sn_2S_3 doped with 8 wt.% Cu.[7,25] Therefore, Cu doping in Sn_2S_3 thin films can improve their electrical properties by increasing their charge carrier density, reducing their resistance and Hall mobility.

I-V Characteristics

I-V characteristic behavior of Cu-doped Sn_2S_3 thin films is shown in Fig. 12. The observed results show ohmic behavior for prepared thin films and confirm that increasing reverse bias voltage linearly increases current generation in the depletion region. Increasing I–V characteristics increase the concentration of Cu up to 4 wt.%; thereafter, it is decreased for further doping. In this study, the variation in I–V characteristics may be attributed to the lattice defects and disordered arrangements on the surface of the film, which can enhance the scattering effect. Based on these results, we can conclude that the thin film's conductivity is increased by Cu ions occupying the Sn_2S_3 lattice and contributing an electron to the conduction band.

CONCLUSION

The structural, morphological, and optical properties of polycrystalline pure and copper-doped tin-sulfide (Cu-Sn_2S_3) thin films were prepared by the spray pyrolysis method. XRD patterns of the Cu-doped Sn_2S_3 correspond to the orthorhombic phase with *Pnma* space group. Doped thin films showed decreased crystallite size due to replacement of larger Sn^{2+} ions being replaced by Cu^{2+} ions. The morphology of Sn_2S_3 thin films shows distribution of loosely packed flattened needle-shaped grains whereas after doping the morphology shows densely packed needle-shaped particles. The band gap values changed with an addition of Cu because of replacement of Sn by Cu, which can introduce the traps and intermediate energy levels. Optical and electrical conductivity changes because of addition of Cu. The optical properties showed that the materials can be engineered by proper doping with Cu. From the I–V measurements, electrical conductivity increased for 2 wt.% and 4 wt.% Cu-doped thin films because of addition of charge carriers, whereas for higher concentration the addition of Cu may create traps for the charge carriers leading to decreased conductivity. From the Hall measurements, the negative value of the Hall coefficient for all the thin films suggests *n*-type semiconductor nature. Further Cu doping in Sn_2S_3 increased the charge carrier density and hence reduced the resistance and Hall mobility.

Therefore, from the optical and electrical measurements it is concluded that Cu-doped Sn_2S_3 thin films exhibit potential features for photovoltaic applications as well as optoelectronics.

SUPPLEMENTARY INFORMATION

The online version contains supplementary material available at https://doi.org/10.1007/s11837-023-06276-6.

ACKNOWLEDGEMENTS

The author Nagaraja BS thanks NMAM Institute of Technology, Nitte, Karkala, Karnataka, India, for

providing the research facilities and encouragement to carry out the study. One of the authors (AR) acknowledges the DST-FIST Grant (SR/FIST/PS-1/2017/8) for the given financial support required to carry out this work. The authors Jayadev and Mahendra thank REVA University for their support in carrying out this work.

AUTHOR CONTRIBUTIONS

BSN: Methodology and writing–reviewing review, original draft (equal), KPG: Methodology and formal analysis and review–editing (equal), KM: Writing–review (equal) and formal analysis and review-editing. JP: Conceptualization, writing–review (equal) and editing, SCG: Methodology and conceptualization, Ravikirana: Characterization facility and conceptualization, AR: Characterization facility and conceptualization, KSP: Conceptualization, writing–review and editing (equal).

DATA AVAILABILITY

All data generated or analyzed during this study are included in this manuscript or are available from the corresponding author on reasonable request.

CONFLICT OF INTEREST

The authors declare that they have no known competing financial interests or personal relationships that could have appeared to influence the work reported in this paper.

REFERENCES

1. S. Joshua Gnanamuthu, I. Kartharinal Punithavathy, S. Johnson Jeyakumar, P.C. Jobe Prabhakar, K. Parasuraman, V.S. Nagarethinam, K. Usharani, and A.R. Balu, *Acta Phys. Pol. A.* 133, 15 https://doi.org/10.12693/APhysPolA.133.15 (2018).
2. J. Kim, J. Kim, S. Yoon, J.-Y. Kang, C.-W. Jeon, and W. Jo, *J. Phys. Chem. C* 122, 3523 https://doi.org/10.1021/acs.jpcc.8b00179 (2018).
3. S.F. Wang, W. Wang, W.K. Fong, Y. Yu, and C. Surya, *Sci. Rep.* 7, 39704 https://doi.org/10.1038/srep39704 (2017).
4. J. David, *Appl. Phys. Lett.* 109, 032102 https://doi.org/10.1063/1.4959104 (2016).
5. A. Mary Saroja, I. Kartharinal Punithavathy, S. Johnson Jeyakumar, A.R. Balu, and S. Joshua Gnanamuthu, *J. Mater. Sci. Mater. Electron.* 28, 11464 https://doi.org/10.1007/s10854-017-6942-2 (2017).
6. L.A. Burton, and A. Walsh, *J. Phys. Chem. C* 116, 24262 https://doi.org/10.1021/jp309154s (2012).
7. J. Srivind, V.S. Nagarethinam, and A.R. Balu, *Mater. Sci. Pol.* 34, 393 https://doi.org/10.1515/msp-2016-0035 (2016).
8. M. Khadraoui, N. Benramdane, C. Mathieu, A. Bouzidi, R. Miloua, Z. Kebbab, K. Sahraoui, and R. Desfeux, *Solid State Commun.* 150, 297 https://doi.org/10.1016/j.ssc.2009.10.032 (2010).
9. D. Avellaneda, I. Sánchez-Orozco, J.A.A. Martínez, S. Shaji, and B. Krishnan, *Mater. Res. Express* 6, 016409 https://doi.org/10.1088/2053-1591/aae3a9 (2018).
10. B. Chen, Xu. Xinhua, F.W.J. Liu, and J. Ji, *Mater. Lett.* 65, 400 https://doi.org/10.1016/j.matlet.2010.10.008 (2011).
11. B.H. Baby, and D.B. Mohan, *Sol. Energy* 189, 207 https://doi.org/10.1016/j.solener.2019.07.059 (2019).
12. L. Motevalizadeh, M. Khorshidifar, M. Ebrahimizadeh Abrishami, and M.M. Bagheri Mohagheghi, *J. Mater. Sci. Mater. Electron.* 24, 3694 https://doi.org/10.1007/s10854-013-1305-0 (2013).
13. H. Kafashan, *Ceram. Int.* 45, 334 https://doi.org/10.1016/j.ceramint.2018.09.172 (2019).
14. M. Patel, and A. Ray, *RSC Adv.* 4, 39343 https://doi.org/10.1039/C4RA06219A (2014).
15. T. Srinivasa Reddy, and M.C. Santhosh Kumar, *RSC Adv.* 6, 95680 https://doi.org/10.1039/C6RA20129F (2016).
16. S. Joshua Gnanamuthu, S. Johnson Jeyakumar, I. Kartharinal Punithavathy, P.C. Jobe Prabhakar, M. Suganya, K. Usharani, and A.R. Balu, *Optik* 127, 3999 https://doi.org/10.1016/j.ijleo.2016.01.112 (2016).
17. O.I. Diaz-Grijalva, D. Berman-Mendoza, A. Flores-Pacheco, R. López-Delgado, A. Ramos-Carrazco, and M.E. Alvarez-Ramos, *J. Mater. Sci. Mater. Electron.* 31, 1722 https://doi.org/10.1007/s10854-019-02690-2 (2020).
18. A.A. Aboud, A. Mukherjee, N. Revaprasadu, and A.N. Mohamed, *J. Mater. Res. Technol.* 8, 2021 https://doi.org/10.1016/j.jmrt.2018.10.017 (2019).
19. D.C. Agarwal, U.B. Singh, S. Gupta, R. Singhal, P.K. Kulriya, F. Singh, A. Tripathi, J. Singh, U.S. Joshi, and D.K. Avasthi, *Sci. Rep.* 9, 6675 https://doi.org/10.1038/s41598-019-43184-9 (2019).
20. A. Sanchez-Juarez, and A. Ortíz, *Semicond. Sci. Technol.* 17, 931 https://doi.org/10.1088/0268-1242/17/9/305 (2002).
21. S. Zhang, and S. Cheng, *Micro Nano Lett.* 6, 559 https://doi.org/10.1049/mnl.2011.0121 (2011).
22. G. Yergaliuly, B. Soltabayev, S. Kalybekkyzy, Z. Bakenov, and A. Mentbayeva, *Sci. Rep.* 12, 851 https://doi.org/10.1038/s41598-022-04782-2 (2022).
23. K.S. Kumar, A.G. Manohari, C. Lou, T. Mahalingam, and S. Dhanapandian, *Vacuum* 128, 226 https://doi.org/10.1016/j.vacuum.2016.04.003 (2016).
24. S. Joshua Gnanamuthu, I. Kartharinal Punithavathy, S. Johnson Jeyakumar, K. Usharani, and A.R. Balu, *Mater. Res. Innov.* 20, 395 https://doi.org/10.1080/14328917.2016.1170321 (2016).
25. A. Mary Saroja, I. Kartharinal Punithavathy, S. Johnson Jeyakumar, S. Joshua Gnanamuthu, and A.R. Balu, *Optik* 130, 245 https://doi.org/10.1016/j.ijleo.2016.08.083 (2017).
26. L. Vegard, *Z. Phys.* 5, 17 https://doi.org/10.1007/BF01349680 (1921).
27. Y. Liu, K. Cao, J. Liu, Z. Zhang, J. Ji, F. Wang, and Z. Li, *J. Mater. Sci. Mater. Electron.* 30, 15880 https://doi.org/10.1007/s10854-019-01924-7 (2019).
28. D. Prabha, S. Ilangovan, V.S. Nagarethinam, and A.R. Balu, *Mater. Res. Innov.* 20, 307 https://doi.org/10.1080/14328917.2015.1134854 (2016).
29. P.R. Bommireddy, C.S. Musalikunta, C. Uppala, and S.H. Park, *Mater. Sci. Semicond. Process.* 71, 139 https://doi.org/10.1016/j.mssp.2017.07.020 (2017).
30. K. Santhosh Kumar, C. Manoharan, S. Dhanapandian, and A. Gowri Manohari, *Spectrochim. Acta A Mol.* 115, 840 https://doi.org/10.1016/j.saa.2013.06.112 (2013).
31. R.N. Mohan, M.T. Nair, and P.K. Nair, *Appl. Surf. Sci.* 504, 144162 https://doi.org/10.1016/j.apsusc.2019.144162 (2020).
32. K. Usha, R. Sivakumar, and C. Sanjeeviraja, *J. Appl. Phys.* 114, 123501 https://doi.org/10.1063/1.4821966 (2013).
33. D. Panda, and T.-Y. Tseng, *Thin Solid Films* 531, 1 https://doi.org/10.1016/j.tsf.2013.01.004 (2013).
34. T. Srinivasa Reddy, and M.C. SanthoshKumar, *Ceram. Int.* 42, 12262 https://doi.org/10.1016/j.ceramint.2016.04.172 (2016).
35. A.A.M. FaragI, and S. Yahia, *Opt. Commun.* 283, 4310 https://doi.org/10.1016/j.optcom.2010.06.081 (2010).

36. B.S. Nagaraja, S.C. Gurumurthy, R. Bairy, K. Ramam, K. Bindu, and A. Rao, *Opt. Mater.* 122, 111669 https://doi.org/10.1016/j.optmat.2021.111669 (2021).
37. M.A. Manthrammel, M. Shkir, S. Shafik, M. Anis, and S. AlFaify, *J. Mater. Res.* 35, 410 https://doi.org/10.1557/jmr.2020.26 (2020).
38. M. Shkir, V. Ganesh, S. Al Faify, and I.S. Yahia, *J. Mater. Sci. Mater. Electron.* 28, 10573 https://doi.org/10.1007/s10854-017-6831-8 (2017).
39. Z.R. Khan, S.M. Munirah, A.S. Alshammari, V. Ganesh, S. AlFaify, and M. Gandouzi, *Thin Films J. Electron. Mater.* 48, 1122 https://doi.org/10.1007/s11664-018-6832-2 (2019).